

Intergalactic dust and its photoelectric heating

Akio K. Inoue* & Hideyuki Kamaya†

Abstract

We have examined the dust photoelectric heating in the intergalactic medium (IGM). The heating rate in a typical radiation field of the IGM is represented by $\Gamma_{\text{pe}} = 1.2 \times 10^{-34} \text{ erg s}^{-1} \text{ cm}^{-3} (\mathcal{D}/10^{-4}) (n_{\text{H}}/10^{-5} \text{ cm}^{-3})^{4/3} (J_{\text{L}}/10^{-21} \text{ erg s}^{-1} \text{ cm}^{-2} \text{ Hz}^{-1} \text{ sr}^{-1})^{2/3} (T/10^4 \text{ K})^{-1/6}$, where \mathcal{D} is the dust-to-gas mass ratio, n_{H} is the hydrogen number density, J_{L} is the mean intensity at the hydrogen Lyman limit of the background radiation, and T is the gas temperature, if we assume the new X-ray photoelectric yield model by Weingartner et al. (2006) and the dust size distribution in the Milky Way by Mathis, Rumpl, & Nordsieck (1977). This heating rate dominates the HI and HeII photoionization heating rates when the hydrogen number density is less than $\sim 10^{-6} \text{ cm}^{-3}$ if $\mathcal{D} = 10^{-4}$ which is 1% of that in the Milky Way, although the heating rate is a factor of 2–4 smaller than that with the old yield model by Weingartner & Draine (2001). The grain size distribution is very important. If only large ($\geq 0.1 \mu\text{m}$) grains exist in the IGM, the heating rate is reduced by a factor of $\simeq 5$. Since the dust heating is more efficient in a lower density medium relative to the photoionization heating, it may cause an inverted temperature–density relation in the low density IGM suggested by Bolton et al. (2008). Finally, we have found that the dust heating is not very important in the mean IGM before the cosmic reionization.

1 Introduction

Dust grains are formed at the end of the stellar life; in the stellar wind of asymptotic giant branch stars (e.g., Ferrarotti & Gail 2006), in the stellar ejecta of supernovae (e.g., Nozawa et al. 2003, Rho et al. 2008), and so on. Some of the grains grow in molecular clouds (e.g., Draine 1990). Some of them are destroyed by the interstellar shock (e.g., Williams, et al. 2006). Some of them may go out from the parent galaxy and reach the intergalactic medium (IGM) (e.g., Aguirre et al. 2001a,b).

The IGM is the medium between galaxies, and it occupies almost the whole volume of the Universe. The mean density of the IGM is as low as 10^{-7} – 10^{-4} cm^{-3} . As found by Gunn & Peterson (1965), the IGM is highly ionized after the cosmic reionization epoch (the redshift $z \simeq 6$ – 10 ; Loeb & Barkana 2001, Fan, Carilli, & Keating 2006). Thus, its temperature is $\sim 10^4 \text{ K}$. The IGM is filled with the ionizing ultra-violet (UV) and X-ray background radiation which is produced by QSOs and galaxies (e.g., Haardt & Madau 1996).

A significant amount of metals is found in the IGM (e.g., Aguirre et al. 2001c). Multiple supernova explosions (SN) caused by an active star-formation in galaxies can eject the metal elements to the IGM. However, Ferrara, Pettini, & Shchekinov (2000) showed that the metal enrichment of the IGM by SN explosions is limited in relatively small regions around star-forming galaxies and an additional physical mechanism is required to explain the observed global enrichment of metals in the IGM. Dust grains expelled from galaxies by the radiation pressure due to stellar light and by the galactic wind due to multiple SNe may contribute to the metal enrichment in the IGM (e.g., Aguirre et al. 2001a,b). Bianchi & Ferrara (2005) showed that relatively large ($> 0.1 \mu\text{m}$) dust grains are not completely destroyed and reach a significant distance (a few $\times 100 \text{ kpc}$) although the amount of this intergalac-

*College of General Education, Osaka Sangyo University, 3-1-1, Nakagaito, Daito, 574-8530 Osaka: akinoue@las.osaka-sandai.ac.jp

†Department of Earth and Ocean Sciences, National Defense Academy of Japan, Hashirimizu 1-10-20, Yokosuka 239-8686, Kanagawa

tic dust is too small to make a detectable extinction.

Infrared (IR) emission from dust grains in the IGM surrounding edge-on galaxies has been already detected (e.g., Alton, Davies, & Bianchi 1999, Bendo et al. 2006). Moreover, IR emission from dust in the IGM accumulated from the distant Universe may affect the cosmic far-infrared background and the cosmic microwave background (Aguirre & Haiman 2000). Emission signature from dust even at the epoch of the cosmic reionization may be detectable with a future satellite observing the cosmic microwave background (Elfgren, Désert, & Guiderdoni 2007).

Xilouris et al. (2006) found a significant reddening of galaxies behind the M81 group IGM which is detected by HI 21 cm emission (e.g., Yun, Ho, & Lo 1994). Their measurements imply the dust-to-gas ratio in the M81 group IGM is a factor of 5 larger than that in the Milky Way. Such a large amount of dust in the IGM may be ejected from M82 by its intense starburst activity (Alton et al. 1999).

Dust in the IGM affects results from the precision cosmology. Indeed, high redshift SNe Ia are dimmed by dust in the IGM, and then, the observational estimate of the distance to them and cosmological parameters become ambiguous (Goobar, Bergström, & Mörtzell 2002). Furthermore, future investigations of the ‘equation of state’ of the Dark energy will be affected by the extinction of the intergalactic dust even if its amount is too small to affect the conclusion of the presence of the Dark energy (Carasanti 2006, Zhang & Corasanti 2007).

Dust in the IGM also affects the thermal history of the IGM. In the intracluster medium, dust grains work as a coolant because they emit energy obtained from gas particles collisionally as the thermal IR radiation (Montier & Giard 2004). Such emission from some nearby galaxy clusters can be detectable with the current and future satellites for the IR observations (Yamada & Kitayama 2005). Dust grains in the IGM also work as a heating source via the photoelectric effect (Nath, Sethi & Shchekinov 1999). Inoue & Kamaya (2003, 2004) proposed a possibility to obtain an upper limit of the amount of the intergalactic dust based on the thermal history of the IGM with the dust photoelectric heating.

In this paper, we revisit the effect of the dust photoelectric heating in the IGM. Recently, Weingartner et al. (2006) revised the model of the photoelectric yield

of dust grains. They included a few new physical processes; the photon and electron transfer in a grain, the photoelectron emission from the inner shells of the constituent atoms of grains, the secondary electron emission, and the Auger electron emission. These new features reduce the photoelectric yield for moderate energy photons of ~ 100 eV but enhance the yield for high energy photons of > 1 keV. In particular, we explore the effect of the new yield model on the photoelectric heating by the intergalactic dust in this paper.

The rest of this paper consists of four sections; in §2, we describe the model of the photoelectric effect. In §3, we compare heating rates of the photoelectric effect with those of the photoionization in the IGM. In §4, we discuss the implications of the results of §3. Final section is devoted for our conclusions.

2 Dust photoelectric effect

2.1 Grain charging processes

To examine the photoelectric effect, we must specify the charge of grains which is given by the following equation (Spitzer 1941, Draine & Salpeter 1979):

$$\frac{dZ_d}{dt} = \sum_i R_i + R_{pe}, \quad (1)$$

where Z_d is the grain charge in the electron charge unit, R_i is the collisional charging rate by i -th charged particle (hereafter the subscript “ i ” means “ i -th charged particle”), and R_{pe} is the photoelectric charging rate. We consider only protons and electrons as the charged particle.

2.1.1 Collisional charging rate

The collisional charging rate by i -th charged particle, R_i , is expressed as (e.g., Draine & Sutin 1987)

$$R_i = Z_i s_i n_i \int_0^\infty \sigma_i(a, Z_d, Z_i, v_i) v_i f(v_i) dv_i, \quad (2)$$

where Z_i is the charge in the electron charge unit, s_i is the sticking coefficient, n_i is the number density, v_i is the velocity, σ_i is the collisional cross section depending on the grain radius, a , both charges, and the velocity, and $f(v_i)$

is the velocity distribution function. If the grain and the charged particle have the charges of the same sign, the kinetic energy of the particle must exceed the grain electric potential for the collision. Otherwise, the collisional cross section is zero. We simply assume s_i is always unity.

Now, we introduce the dimensionless cross section, $\tilde{\sigma}_i = \sigma_i/\pi a^2$. If we neglect the “image potential” resulting from the polarization of the grain induced by the Coulomb field of the approaching charged particle (Draine & Sutin 1987) and we assume the Maxwellian velocity distribution for the particle and the spherical grains, we obtain

$$\int_0^\infty \tilde{\sigma}_i v_i f(v_i) dv_i = \left(\frac{8k_B T}{\pi m_i} \right)^{1/2} g(x), \quad (3)$$

and

$$g(x) = \begin{cases} 1 - x & \text{for } Z_d Z_i \leq 0 \\ \exp(-x) & \text{for } Z_d Z_i > 0 \end{cases}, \quad (4)$$

where k_B is the Boltzmann’s constant, T is the gas temperature, m_i is the particle mass, and $x = e^2 Z_d Z_i / a k_B T$ (Spitzer 1941).

In fact, the “image potential” works to enhance the collisional cross section (Draine & Sutin 1987). Although the effect becomes the most important for grains with an around neutral charge, it quickly declines for highly charged grains. Indeed, for the charge ratio of $Z_d/Z_i < -3$, which is satisfied in our case as found below, the increment factor for the cross section by the effect of the “image potential” is less than 1.5 (Draine & Sutin 1987). Therefore, we neglect the “image potential” in this paper.

2.1.2 Photoelectric charging rate

The photoelectric charging rate is given by (e.g., Draine 1978)

$$R_{pe} = \pi a^2 \int_0^\infty Q_\nu(a) Y_\nu(a, Z_d) \frac{4\pi J_\nu}{h\nu} d\nu, \quad (5)$$

where Q_ν is the absorption coefficient of grains at the frequency ν , Y_ν is the photoelectric yield, J_ν is the mean intensity of the incident radiation, and h is the Planck constant. For Q_ν , we adopt the values of “graphite” and “UV smoothed astronomical silicate” by Draine (2003). If the photon energy is smaller than the threshold energy of the

photoelectric emission, e.g., the ionization potential or the work function, the yield $Y_\nu = 0$.

We adopt a sophisticated model of the photoelectric yield by Weingartner & Draine (2001) and Weingartner et al. (2006) in this paper. The model of Weingartner & Draine (2001) (hereafter WD01 model) takes into account the primary photoelectron emission from the band structure of grains, a small-size particle effect, and the energy distribution of the photoelectron. On the other hand, Weingartner et al. (2006) (hereafter W+06 model) add the primary photoelectron emission from inner shells of the constituent atoms of grains, the Auger electron emission, and the secondary electron emission produced by primary electrons and Auger electrons. The transfer of photons absorbed and electrons emitted in a grain is also taken into account. The detailed procedure of the yield calculations is referred to the original papers of Weingartner & Draine (2001) and Weingartner et al. (2006). Fig. 1 shows comparisons between the WD01 and W+06 models. The reduction of the W+06 yield around 100 eV is due to the effect of the photon/electron transfer in a grain. The W+06 yield exceeds unity for some cases because of the Auger and secondary electrons.

We have to note that there is still a large uncertainty of photoelectric yield models because of our insufficient understandings of the nature of small-size particle effect as well as the lack of experiments. Abbas et al. (2006) reported measurements of the yield of individual grains of silica, olivine, and graphite with 0.09–5 μm radii for 8–10 eV photons. Their measurements indeed show larger yields than those of the bulk materials. However, the measurements do not agree with the yield enhancement factors adopted in WD01 and W+06 models accounting for the small-size particle effect qualitatively as well as quantitatively. Clearly, we need more experiments and theoretical investigations of the photoelectric yield in future.

2.1.3 Equilibrium charge

We need to specify the radiation field incident on grains in the IGM: the cosmic background radiation. We assume a simple prescription of the radiation. The intensity of the radiation at the Lyman limit is estimated from observations of the proximity effect and the Lyman α forest opacity (e.g., Scott et al. 2000). A typical value of the intensity at the Lyman limit is $J_L = 1 \times 10^{-21}$ erg s $^{-1}$

$\text{cm}^{-2} \text{Hz}^{-1} \text{sr}^{-1}$ (e.g., Scott et al. 2000). We simply assume a power-law as the spectral shape: $J_\nu \propto \nu^{-p}$. A typical value of p is unity (e.g., Haardt & Madau 1996). With such a radiation field, the grains in the IGM are positively charged.

A typical charging time-scale is very short. For example, the collisional charging rate of electron, $R_e \sim 5.6 \times 10^{-6} \text{s}^{-1}$ for $n_e = 10^{-5} \text{cm}^{-3}$, $T = 10^4 \text{K}$, $a = 0.1 \mu\text{m}$, and $Z_d = 1700$, which is the equilibrium charge of graphite or silicate grains for these parameters and $J_\nu = 10^{-21}(\nu/\nu_L)^{-1} \text{erg s}^{-1} \text{cm}^{-2} \text{Hz}^{-1} \text{sr}^{-1}$. Thus, the typical charging time-scale is $t \sim 1/R_e \sim 6 \times 10^{-3} \text{yr}$. Therefore, the grain charge can be in equilibrium. We set $dZ_d/dt = 0$ in equation (1) and obtain the equilibrium charge of the IGM grains.

2.2 Heating rates

2.2.1 Heating rate per a grain

The net heating rate per a grain with the radius a is expressed as (e.g., Weingartner & Draine 2001)

$$\gamma(a) = R_{\text{pe}}\mathcal{E}_{\text{pe}}(a) - |R_e|\mathcal{E}_e(T), \quad (6)$$

where $\mathcal{E}_{\text{pe}}(a)$ is the mean kinetic energy of photoelectrons from a grain with the radius a and $\mathcal{E}_e(T)$ is that of electrons colliding with the grain. The second term accounts for the cooling by the electron capture. If we assume the Maxwellian velocity distribution for the electrons, $\mathcal{E}_e(T) = k_B T(2 + \phi)/(1 + \phi)$, where $\phi = Z_d e^2 / a k_B T$ (for $Z_d > 0$; Draine 1978). We note that \mathcal{E}_e is $\sim 1\%$ of \mathcal{E}_{pe} in the current setting.

The mean energy of the photoelectrons is given by

$$\mathcal{E}_{\text{pe}}(a) = \frac{\pi a^2}{R_{\text{pe}}} \int_0^{\nu_{\text{max}}} Q_\nu(a) Y E_\nu(a, Z_d) \frac{4\pi J_\nu}{h\nu} d\nu, \quad (7)$$

and

$$Y E_\nu(a, Z_d) = \sum_k Y_\nu^k(a, Z_d) \langle E_e \rangle_\nu^k(a, Z_d), \quad (8)$$

where Y_ν^k is the photoelectric yield of k -th emission process, e.g., primary electrons from the band structure, Auger electron, etc., and $\langle E_e \rangle_\nu^k$ is the mean energy of electrons emitted by k -th process with the absorbed photon energy $h\nu$. The estimation of $\langle E_e \rangle_\nu^k$ is based on the

assumed energy distribution of the electrons. Following Weingartner et al. (2006), we adopt a parabolic function for the primary and the Auger electrons and a function introduced by Draine & Salpeter (1979) for the secondary electrons, which were derived to fit some experimental results.

In the IGM, the grains are positively charged. Then, the proton collisional charging rate is negligible. Thus, the photoelectric charging rate balances with the electron collisional charging rate: $R_{\text{pe}} + R_e = 0$. In this case, equation (6) is reduced to

$$\begin{aligned} \gamma(a) &= |R_e|(\mathcal{E}_{\text{pe}} - \mathcal{E}_e) \\ &\approx \pi a^2 n_e \left(\frac{8k_B T}{\pi m_e} \right)^{1/2} \left(\frac{eV_d}{k_B T} \right) \mathcal{E}_{\text{pe}}, \quad (9) \end{aligned}$$

where we have used equations (2–4) for R_e and $V_d = Z_d e/a$ is the grain electric potential ($eV_d/k_B T \gg 1$ and $\mathcal{E}_{\text{pe}} \gg \mathcal{E}_e$ for the IGM). As found later in Fig. 2, the electric potential depends on the grain size weakly in the W+06 yield case. We confirmed that the mean energy of photoelectrons also depends on the grain size weakly. As a result, the heating rate per a grain is roughly proportional to the square of the size, which is shown later in Fig. 3.

2.2.2 Total photoelectric heating rate

To estimate the total photoelectric heating rate per unit volume, we need to specify the amount and the size distribution of dust grains. A power law type distribution for grain size is familiar in the interstellar medium of the Milky Way since classical work by Mathis, Rumpl, & Nordsieck (1977; hereafter MRN). Power law is expected to be achieved by resulting from coagulation, shattering, and sputtering processes (e.g., Jones, Tielens, & Hollenbach 1996). Here we express the power law distribution as $n(a) = Aa^{-q}$, where $n(a)da$ is the number density of grains with the radius between a and $a + da$. For the MRN distribution, $q = 3.5$ (see Table 1). The normalization A is determined from the total dust mass density $\rho_d = \int_{a_{\text{min}}}^{a_{\text{max}}} m(a)n(a)da$, where $m(a) = (4\pi/3)\rho a^3$ is the mass of grains with the radius a , ρ ($\simeq 3 \text{g cm}^{-3}$) is the grain material density, a_{min} and a_{max} are the minimum and maximum radius, respectively. The dust mass density ρ_d is given by $\rho_d = m_p n_H \mathcal{D}$, where m_p is the

proton mass, n_{H} is the hydrogen number density, and \mathcal{D} is the dust-to-gas mass ratio. We assume $\mathcal{D} = 10^{-4}$, which is about two orders of magnitude smaller than that in the Milky Way's ISM. Then, the total photoelectric heating rate is

$$\Gamma_{\text{pe}} = \int_{a_{\text{min}}}^{a_{\text{max}}} \gamma(a)n(a)da. \quad (10)$$

Let us consider a typical size for the total heating rate. Using the grain number density $n_{\text{d}} = \int_{a_{\text{min}}}^{a_{\text{max}}} n(a)da$, we can define a mean heating rate per a grain as $\langle \gamma \rangle \equiv \int_{a_{\text{min}}}^{a_{\text{max}}} \gamma(a)n(a)da/n_{\text{d}}$ and a mean mass per a grain as $\langle m_{\text{d}} \rangle \equiv \rho_{\text{d}}/n_{\text{d}} = \int_{a_{\text{min}}}^{a_{\text{max}}} m(a)n(a)da/n_{\text{d}}$. Then, the total heating rate is reduced to $\Gamma_{\text{pe}} = \langle \gamma \rangle n_{\text{d}} = \langle \gamma \rangle \rho_{\text{d}} / \langle m_{\text{d}} \rangle$. The heating rate per a grain can be approximated to $\gamma(a) \approx \gamma_0 a^2$ as seen in §2.2.1 (see also Fig. 3 and §3.1.2), where γ_0 is a normalization. The grain mass is $m(a) = (4\pi/3)\rho a^3$. Then, we obtain

$$\Gamma_{\text{pe}} \approx \frac{3\rho_{\text{d}}\gamma_0}{4\pi\rho\langle a \rangle}, \quad (11)$$

where a typical size $\langle a \rangle$ is given by

$$\langle a \rangle = \frac{\int_{a_{\text{min}}}^{a_{\text{max}}} a^3 n(a)da}{\int_{a_{\text{min}}}^{a_{\text{max}}} a^2 n(a)da}. \quad (12)$$

Note that a larger typical size results in a smaller total heating rate because of a smaller number density of grains for a fixed dust mass.

2.2.3 Photoionization heating rates

For comparison with the photoelectric heating rate by grains, we estimate the photoionization heating rates of hydrogen and helium. The net HI photoionization heating rate is

$$\Gamma_{\text{pi}}^{\text{HI}} = n_{\text{HI}}R_{\text{pi}}^{\text{HI}}\mathcal{E}_{\text{pi}}^{\text{HI}} - n_{\text{HII}}R_{\text{re}}^{\text{HI}}\mathcal{E}_{\text{gas}}, \quad (13)$$

where $R_{\text{pi}}^{\text{HI}} = \int_{\nu_{\text{L}}^{\text{HI}}}^{\infty} \sigma_{\nu}^{\text{HI}} 4\pi J_{\nu} / h\nu d\nu$ is the HI photoionization rate, $R_{\text{re}}^{\text{HI}} = n_{\text{e}}\alpha_{\text{A}}^{\text{HI}}(T)$ is the HI recombination rate, $\mathcal{E}_{\text{pi}}^{\text{HI}} = (1/R_{\text{pi}}^{\text{HI}}) \int_{\nu_{\text{L}}^{\text{HI}}}^{\infty} \sigma_{\nu}^{\text{HI}} 4\pi J_{\nu} / h\nu (h\nu - h\nu_{\text{L}}^{\text{HI}}) d\nu$ is the mean kinetic energy of the HI photoionized electrons, σ_{ν}^{HI} is the HI photoionization cross section, $\nu_{\text{L}}^{\text{HI}}$ is the HI Lyman limit frequency, n_{HI} , n_{HII} , and n_{e} are the neutral hydrogen, ionized hydrogen, and electron number densities,

respectively, $\alpha_{\text{A}}^{\text{HI}}(T)$ is the Case A HI recombination coefficient for the gas temperature T (Osterbrock & Ferland 2006), and \mathcal{E}_{gas} is the mean kinetic energy lost from the gas per one recombination. If we assume that $J_{\nu} \propto \nu^{-p}$ and $\sigma_{\nu}^{\text{HI}} \propto \nu^{-3}$, we obtain $\mathcal{E}_{\text{pi}}^{\text{HI}} = h\nu_{\text{L}}^{\text{HI}} / (p + 2)$. If we take into account the gas cooling by free-free emission, $\mathcal{E}_{\text{gas}} \approx k_{\text{B}}T$ for the Case A and $T = 10^4$ K (Osterbrock & Ferland 2006). If we assume the ionization equilibrium, $n_{\text{HI}}R_{\text{pi}}^{\text{HI}} = n_{\text{HII}}R_{\text{re}}^{\text{HI}}$, we obtain

$$\Gamma_{\text{pi}}^{\text{HI}} = n_{\text{H}}^2 \alpha_{\text{A}}^{\text{HI}}(T) (\mathcal{E}_{\text{pi}}^{\text{HI}} - \mathcal{E}_{\text{gas}}), \quad (14)$$

where we have assumed $n_{\text{HII}} = n_{\text{e}} = n_{\text{H}}$ with n_{H} being the hydrogen number density, that is, the neutral fraction is assumed to be very small. The net HeII photoionization heating rate is likewise

$$\Gamma_{\text{pi}}^{\text{HeII}} = n_{\text{He}}n_{\text{H}}\alpha_{\text{A}}^{\text{HeII}}(T) (\mathcal{E}_{\text{pi}}^{\text{HeII}} - \mathcal{E}_{\text{gas}}), \quad (15)$$

n_{He} is the helium number density, $\alpha_{\text{A}}^{\text{HeII}}(T)$ is the HeII recombination rate, and $\mathcal{E}_{\text{pi}}^{\text{HeII}}$ is the mean kinetic energy of the HeII photoionized electrons. We assume $n_{\text{He}}/n_{\text{H}} = 0.1$.

3 Results

3.1 Comparison between the two yield models

We compare the grain charge and heating rates with the WD01 and W+06 models quantitatively in the IGM environment. Weingartner et al. (2006) showed the grain charges in QSO environments which are similar situation with a similar radiation field in this paper. However, they did not show the heating rates in the environment.

3.1.1 Electric potential

In Fig. 2, we compare the electric potentials of the W+06 model (solid lines) with those of the WD01 model (dashed lines). We showed two cases of the spectrum of the radiation field; one has a hard spectrum as a background radiation dominated by QSOs which is the case with the spectral index $p = 1$, and the other has a soft spectrum with $p = 5$ for a comparison. Other assumed quantities are appropriate for the IGM at the redshift $z \sim 3$ and shown in

the panels. The radiation fields assumed here correspond to the ionization parameter $U \equiv n_{\text{ion}}/n_{\text{H}}$, which is the number density ratio of ionizing photons and hydrogen nucleus, of 6.3 for $p = 1$ and of 1.3 for $p = 5$. Weingartner et al. (2006) showed electric potentials in their Figs. 6 and 7 with $U = 0.1\text{--}100$. We find that our calculations are quantitatively well matched with theirs.

We find in Fig. 2 that for the hard spectrum case, the grain electric potentials with the W+06 yield model are much smaller than those with the WD01 model, especially for larger grain sizes. On the other hand, for the soft spectrum case, the difference is very small, less than 4%. This is because the main difference between the W+06 yield and the WD01 yield is found in the primary photoelectron yield at ~ 100 eV due to the photon/electron transfer in a grain as shown in Fig. 1. In the soft spectrum case, since there are not many photons around the energy, we do not find a significant difference between the two yield models. For smaller grain sizes, the yield reduction by the photon/electron transfer is small as found in Figs. 4 and 5 of Weingartner et al. (2006). Thus, we do not find a significant difference in the electric potentials for smaller grain sizes in Fig. 2, either.

The electrostatic stress on a grain may cause the grain destruction by the Coulomb explosion (e.g., Draine & Salpeter 1979). The critical electric potential is $V_{\text{max}} = 1063 \text{ V} (S_{\text{d}}/10^{10} \text{ dyn cm}^{-2})^{1/2} (a/0.1 \mu\text{m})$, where S_{d} is the tensile strength of grains, which is very uncertain. Perfect crystal structure may have $S_{\text{d}} \sim 10^{11} \text{ dyn cm}^{-2}$ (Draine & Salpeter 1979), but imperfections would reduce the strength as $S_{\text{d}} \sim 10^{10} \text{ dyn cm}^{-2}$ (Fruchter et al. 2001). Following Weingartner et al. (2006), we show two cases of the critical potential with $S_{\text{d}} \sim 10^{10}$ and $10^{11} \text{ dyn cm}^{-2}$ in Fig. 2 as the dotted lines. The critical potential by the ion field emission is similar to the case with $S_{\text{d}} \sim 10^{11} \text{ dyn cm}^{-2}$ (Draine & Salpeter 1979). We find that grains smaller than 20–30 Å in the hard radiation field may be destroyed by the Coulomb explosion. Then, there may be no very small grains in the IGM.

3.1.2 Photoelectric heating rate

Fig. 3 shows the photoelectric heating rate per a grain in a typical $z \sim 3$ IGM environment with a hard radiation; graphite grains are shown by solid lines and silicate grains are shown by the dashed lines. In the panel (a), we show

the absolute value of the heating rate for the W+06 yield model. As expected in equation (9), the heating rate is nicely proportional to a^2 , square of the size. However, the slope becomes gradually steep for a small (< 100 Å) grain size.

In the panel (b), we compare the two heating rates with the W+06 model and the WD01 model. We find that the heating rate with the W+06 model is much smaller than that with the WD01 model: a factor of 10 smaller for the largest grain size. This is because (1) reduction of the grain electric potential and (2) reduction of the mean energy of the photoelectron in the W+06 model. As found in equation (9), the heating rate per a grain is proportional to the product of the potential and the mean photoelectron energy. As seen in Fig. 2, the W+06 model expects smaller potential because of the reduction of the yield at ~ 100 eV. The yield reduction also causes the reduction of the mean energy of the photoelectron as expected in equation (8). Therefore, we have up to about a factor of 10 reduction of the heating rate with the W+06 model.

Fig. 4 shows a comparison of the total heating rates by the W+06 model (solid lines) and by the WD01 model (dotted lines). The horizontal axis is the assumed hydrogen number density. We also show the redshift at which the number density on the horizontal axis corresponds to the mean density of the Universe. We have assumed the MRN grain size distribution (see Table 1). We find that the total heating rate with the W+06 yield is a factor of 2–4 smaller than that with the WD01 yield.

For a comparison, we also show the HI and HeII photoionization heating rates in Fig. 4. We have assumed the ionization equilibrium for them. When we assume the dust-to-gas ratio in the IGM is 1% of that in the Milky Way (i.e. $\mathcal{D} = 10^{-4}$), the dust photoelectric heating dominates the HI and HeII photoionization heatings if the hydrogen number density is less than $10^{-6}\text{--}10^{-5} \text{ cm}^{-3}$ which correspond to the redshift $z \sim 1\text{--}2$. We note that the dust heating is the most important mechanism in the IGM at $z = 0$ even with the W+06 yield model if the IGM has dust with 1% dust-to-gas ratio of the Milky Way and with the MRN size distribution.

3.2 Effect of the grain size distribution

The size distribution of the intergalactic dust grains should be important for the photoelectric heating rate via

the typical size defined by equation (12). However, it is quite uncertain. Thus, we examine several possibilities of the size distribution in this section. Table 1 is a summary of the size distribution considered here.

The grain size distribution in the Milky Way has been approximated to be a power-law since Mathis et al. (1977) suggested as $n(a) \propto a^{-q}$ with $q = 3.5$. This MRN distribution is a reference case and is already adopted in Fig. 4. During the grain transport from galaxies to the IGM, there may be size filtering mechanisms. For example, Ferrara et al. (1991) showed that sputtering in the hot gas filling the galactic halo efficiently destroys grains smaller than $\sim 0.1 \mu\text{m}$. Bianchi & Ferrara (2005) also showed that only grains larger than $\sim 0.1 \mu\text{m}$ reach a significant distance (a few $\times 100$ kpc) from the parent galaxies by calculating the grain ejection by the radiation pressure and the grain destruction by the sputtering simultaneously. Here, we consider a simple size distribution of the MRN with $\geq 0.1 \mu\text{m}$ grains as the BF05 model.

In the early Universe, the dominant source of dust grains is different from that in the current Milky Way. Although asymptotic giant branch stars are considered to be the main dust source in the Milky Way (e.g., Dwek 1998), there is not enough time for stars to evolve to the phase in the early Universe at the redshift $z > 6$. However, a plenty of dust is found in QSOs at $z > 6$ (Bertoldi et al. 2003). SNe are the candidate of the dust source in the early Universe (e.g., Nozawa et al. 2003) and the observed extinction curve of dust associated with the QSO is compatible with those expected from the grains produced by SNe (Maiolino et al. 2004, Hirashita et al. 2005, 2008). Thus, we consider the size distribution expected from the SNe dust production model by Nozawa et al. (2003) as the N03 model. In addition, we adopt the size distribution expected by Nozawa et al. (2007), who explored the effect of the dust destruction by the reverse shock in the SN remnant, as the N07 model.

Finally, we adopt a hypothetical size distribution consisting of only small grains as a comparison case; the MRN distribution with the maximum size of 250 \AA as the SG (small grain) model.

Fig. 5 shows a comparison of total heating rates with the five size distributions considered here. All the cases are assumed the W+06 yield model and physical conditions appropriate for the IGM. The case of the BF05 model (triple-dot-dashed line) is a factor of $\simeq 5$ smaller

than that of the MRN model (thick solid line). This reduction factor is simply accounted for by the ratio of the typical sizes of the two models: $0.16 \mu\text{m}$ for the BF05 model and 350 \AA for the MRN model (see Table 1). The same thing is true for the N07 model (dotted line) and the SG model (thin solid line). The result of the N03 model (dashed line) coincides with that of the MRN model because their typical sizes are similar. In any case, we have a smaller number of grains for a larger typical size if the total dust mass is fixed. Then, the heating rate is reduced. We note that the dust photoelectric heating is still dominant or important mechanism relative to the HI and HeII photoionization heatings in the $z = 0$ IGM even with the BF05 model if the dust-to-gas ratio in the IGM is 1% of that in the Milky Way.

3.3 A simple formula of the dust photoelectric heating rate

Fig. 6 shows the effect of different settings of the calculation on the dust photoelectric heating rate: (a) various intensities of the background radiation and (b) various temperatures of the gas. The W+06 yield model and the MRN size distribution are assumed. We also assume that the dust consists of a mixture of graphite and silicate with the mass ratio of 1:1. The spectral index of the background radiation is always set unity. In the weakest intensity case (squares in the panel [a]), the equilibrium charges for smallest grains ($< 0.01 \mu\text{m}$) are less than 3 in the electric charge unit for the hydrogen density $n_{\text{H}} > 2 \times 10^{-5} \text{ cm}^{-3}$. In these cases, the effect of the ‘‘image potential’’ (Draine & Sutin 1987) is not negligible, then, the current calculations are no longer valid. We note that all the cases shown in Fig. 6 have an equilibrium charge much larger than 3 for all grains in the size distribution.

The resultant heating rates are well expressed as

$$\begin{aligned} \Gamma_{\text{pe}} &= 1.2 \times 10^{-34} \text{ erg s}^{-1} \text{ cm}^{-3} \\ &\times \left(\frac{\mathcal{D}}{10^{-4}} \right) \left(\frac{n_{\text{H}}}{10^{-5} \text{ cm}^{-3}} \right)^{4/3} \left(\frac{T}{10^4 \text{ K}} \right)^{-1/6} \\ &\times \left(\frac{J_{\text{L}}}{10^{-21} \text{ erg s}^{-1} \text{ cm}^{-2} \text{ Hz}^{-1} \text{ sr}^{-1}} \right)^{2/3} \quad (16) \end{aligned}$$

which is shown in Fig. 6 as solid lines. The indices in this formula can be derived analytically follow-

ing Inoue & Kamaya (2004). From eqs. (A4) and (A7) in Inoue & Kamaya (2004), we find $\Gamma_{\text{pe}} \propto J_{\text{L}}^{2/(p+\beta+1)} n_{\text{H}}^{2-2/(p+\beta+1)} T^{3/2-(2p+2\beta+1)/(p+\beta+1)}$, where β is the emissivity (or absorption) index of the dust: $Q_{\nu} \propto \nu^{-\beta}$. Here, we have $p = 1$ and $\beta \approx 1$, then, we obtain the indices in eq. (16).

The deviation of the heating rates from the formula for $T = 10^5$ K and $n_{\text{H}} > 2 \times 10^{-5} \text{ cm}^{-3}$ is due to the relative significance of the cooling by the electron capture (see eq. [6]). Indeed, we find that the mean energy of photoelectrons from small ($< 0.01 \mu\text{m}$) graphite grains is smaller than the mean kinetic energy of the 10^5 K gas in the case of $n_{\text{H}} = 10^{-4} \text{ cm}^{-3}$, then, the net heating rate per such a graphite grain is negative. Thus, we have a reduction of the total heating rate for $T = 10^5$ K and $n_{\text{H}} > 2 \times 10^{-5} \text{ cm}^{-3}$ as found in Fig. 6 (b) although the heating rate by silicate grains is still positive.

The validity of the formula presented in equation (16) is ensured for $n_{\text{H}} = 10^{-7}$ – 10^{-4} cm^{-3} , $J_{\text{L}} = 10^{-23}$ – $10^{-20} \text{ erg s}^{-1} \text{ cm}^{-2} \text{ Hz}^{-1} \text{ sr}^{-1}$, and $T = 10^3$ – 10^5 K within a uncertainty of 30%, except for $n_{\text{H}} > 2 \times 10^{-5} \text{ cm}^{-3}$ with $J_{\text{L}} = 10^{-23} \text{ erg s}^{-1} \text{ cm}^{-2} \text{ Hz}^{-1} \text{ sr}^{-1}$ or $T = 10^5$ K. Note that there may be much larger uncertainty in the photoelectric yield model. If one likes another size distribution rather than the standard MRN, for example the BF05 model discussed in §3.3, the heating rate might be scaled by a factor found in Fig. 5 or the ratio of the typical sizes in Table 1.

4 Discussions

4.1 Amount of the intergalactic dust

Inoue & Kamaya (2003,2004) discussed the effect of the photoelectric heating by the intergalactic dust on the thermal history of the IGM, and then, obtained an upper limit of the intergalactic dust amount. However, we have already seen that the W+06 yield model results in a factor of 2–4 reduction of the photoelectric heating rate relative to the WD01 model which was adopted in Inoue & Kamaya (2003,2004). We can conclude that the upper limits obtained from the IGM thermal history are raised by a few factor. Even in this case, the final limit obtained by Inoue & Kamaya (2004), which is that the intergalactic dust mass should be less than 10% of the metal mass pro-

duced in galaxies, is not affected because the limit was obtained mainly from the reddening measurements of SNe Ia at $z = 0.5$, especially for $\sim 0.1 \mu\text{m}$ size grains.

4.2 Can grains cause an inverted temperature–density relation in the IGM?

Bolton et al. (2008) recently suggest an inverted temperature–density relation in the low density IGM at $z = 2$ – 3 . Previously the temperature in the low density IGM is thought to be proportional to the density positively (e.g., Hui & Gnedin 1997). However, Bolton et al. (2008) examined carefully the probability distribution function (PDF) of the flux in QSOs’ spectra through the Lyman α forest in the IGM, and found that the observed PDF is explained better by the negatively proportional temperature–density relation; lower density IGM is hotter. This needs a more efficient heating source for lower density IGM. Bolton et al. (2008) suggested a radiation transfer effect (e.g., Abel & Haehnelt 1999) for the mechanism.

The intergalactic dust may contribute to the heating in the low density IGM. As shown in Figs. 4 and 5, the importance of the dust photoelectric heating increases in lower density medium which is plausible for the inverted temperature–density relation. For example, we expect a factor of ~ 2 larger heating rate by dust than HeII photoionization heating in a medium with 1/10 of the mean density at $z = 2$ for the MRN size distribution and 1% dust-to-gas ratio of the Milky Way. Thus, the dust photoelectric heating may cause the inverted temperature–density relation observed in the low density IGM at $z = 2$ – 3 . This point should be examined further by implementing the dust heating in a cosmological hydrodynamics simulation. For this, the formula presented in equation (16) will be useful.

4.3 Photoelectric effect before the cosmic reionization

Finally, we examine if the dust photoelectric heating is efficient in the IGM before the cosmic reionization. Because of the prominent Gunn–Peterson trough in QSOs’ spectra (e.g., Fan et al. 2006), the cosmic reionization epoch should be at $z > 6$. Here we consider the IGM

at $z \sim 10$.

Before the reionization, the ionizing background radiation does not exist although a nonionizing UV background can be established by primordial galaxies or active blackhole–accretion disk systems. An X-ray background radiation may also exist (e.g., Venkatesan et al. 2001). We consider two cases; one is the case with only nonionizing UV background radiation and the other is the case with additional X-ray background radiation. For simplicity, we assume the background radiation to be a power-law with the spectral index $p = 1$ and the intensity at the Lyman limit $J_L = 1 \times 10^{-21} \text{ erg s}^{-1} \text{ cm}^{-2} \text{ Hz}^{-1} \text{ sr}^{-1}$. However, we assume no intensity between $E_{\text{UV}}^{\text{max}} = 13.6 \text{ eV}$ and $E_{\text{X}}^{\text{min}} = 300 \text{ eV}$. Thus, in the nonionizing UV only case, we have the background radiation only below $E_{\text{UV}}^{\text{max}} = 13.6 \text{ eV}$. In the case with the X-ray background, we have radiation below $E_{\text{UV}}^{\text{max}} = 13.6 \text{ eV}$ and above $E_{\text{X}}^{\text{min}} = 300 \text{ eV}$. The dust-to-gas ratio in the IGM at $z \sim 10$ is of course unknown, but we assume 1% dust-to-gas ratio of the Milky Way as an example, i.e. $\mathcal{D} = 10^{-4}$. Note that the results obtained in the following discussions are linearly scaled by the value of \mathcal{D} . The mean hydrogen density in the Universe at $z \sim 10$ is $3 \times 10^{-4} \text{ cm}^{-3}$. Table 2 is a summary of the assumed quantities and results obtained below.

In the nonionizing UV radiation only case, there is no efficient heating mechanism for the whole of the Universe although primordial objects can heat up their surrounding gas locally. Thus, the temperature of the gas far away the sources is kept to be that of the cosmic background radiation at the epoch: $\sim 30 \text{ K}$. The electron fraction x_e , i.e. the number density of electron relative to that of hydrogen nucleus, is $\sim 10^{-4}$ in this low temperature IGM (Galli & Palla 1998). The nonionizing UV photons still cause the photoelectric effect of grains. In the assumed setting, we have found that grains are positively charged and the dust photoelectric heating rate becomes $\Gamma_{\text{pe}} \simeq 7 \times 10^{-36} \text{ erg s}^{-1} \text{ cm}^{-3}$ for the MRN size distribution with a graphite and silicate mixture (50% each in mass). We compare this heating rate with the gas thermal energy density: $U_{\text{gas}} = (3/2)n_{\text{H}}k_{\text{B}}T$. The time-scale doubling the gas temperature with the photoelectric heating is given by $t_{\text{pe}} \equiv U_{\text{gas}}/\Gamma_{\text{pe}} \simeq 9 \times 10^9 \text{ yr}$. Since the age of the Universe at $z = 10$ is about $5 \times 10^8 \text{ yr}$, we conclude that the dust photoelectric heating is not very efficient in this case although it may be the strongest heating mecha-

nism for the IGM.

In the case with the additional X-ray background radiation, the IGM is partially ionized by the X-ray and the temperature becomes $\sim 10^4 \text{ K}$ (e.g., Venkatesan et al. 2001). If we assume the ionization equilibrium and optically thin for the X-ray, the electron fraction becomes $x_e \simeq 0.3$ for the current setting of the X-ray background. In this medium, the grains are positively charged and the dust photoelectric heating rate becomes $\Gamma_{\text{pe}} \simeq 2 \times 10^{-33} \text{ erg s}^{-1} \text{ cm}^{-3}$. We have assumed the MRN size distribution with a graphite and silicate mixture (50% each in mass), again. However, the HI photoionization heating is much more efficient as $\Gamma_{\text{pi,X}}^{\text{HI}} \simeq 2 \times 10^{-30} \text{ erg s}^{-1} \text{ cm}^{-3}$. Therefore, we again conclude that the dust photoelectric heating is negligible in the early Universe filled with an X-ray background radiation.

5 Conclusion

We have updated our calculations made in Inoue & Kamaya (2003,2004) of the dust photoelectric heating in the IGM with the new model of the dust photoelectric yield by Weingartner et al. (2006). This new yield model takes into account the effect of the photon and electron transfer in a grain, the photoelectric emission from inner shells of grain constituent atoms, the Auger electron emission, and the secondary electron emission. A comparison with the previous yield model by Weingartner & Draine (2001) show that the new yield is smaller than the old one for $\sim 100 \text{ eV}$ photons. This reduction of the yield is due to the photon/electron transfer effect, and reduces the electric potential on grains and the heating rate significantly. For example, if we integrate over the grain size with the standard MRN distribution, the dust photoelectric heating rate with the new yield model is a factor of 2–4 smaller than that with the old yield model. The photoelectric heating rate is more important in lower density medium. If the dust-to-gas ratio in the IGM is 1% of that in the Milky Way and the size distribution is the standard MRN model, the dust heating rate dominates the HI and HeII photoionization heating rates when the gas number density is less than $\sim 10^{-6} \text{ cm}^{-3}$ even with the new yield model.

We have examined the effect of the size distribution function on the heating rate because the heating rate is inversely proportional to the typical grain size as found in

equation (11). Bianchi & Ferrara (2005) suggested that the size of the intergalactic dust is larger than $\sim 0.1 \mu\text{m}$ because smaller grains are destroyed by sputtering in the hot gas halo during the transport of grains from the parent galaxy to the IGM. In this case, the heating rate is reduced by a factor of ~ 5 relative to that with the standard MRN size distribution. The size distributions expected by the dust formation model in supernova ejecta are also examined. The heating rate with the size distribution of the grains just produced in the ejecta is very similar to that with the MRN distribution. In contrast, the heating rate with the size distribution of the grains processed by the reverse shock in the supernova remnant is a factor of ~ 3 smaller than that with the MRN model. The shock processed grains have larger size than the pristine ones because smaller grains are destroyed. On the other hand, if we put only small grains in the IGM, the heating rate increases significantly. Therefore, we conclude that the size distribution of grains in the IGM is an essential parameter for determining the dust heating efficiency. Even in the worst case considered here, the dust heating is expected to be the dominant heating mechanism in the IGM at $z = 0$ if the dust-to-gas ratio in the IGM is 1% of that in the Milky Way.

Since the dust photoelectric heating rate with the new yield model is reduced by a factor of 2–4 relative to that with the old yield model, the upper limit on the amount of the intergalactic dust obtained by Inoue & Kamaya (2003, 2004) may be affected. Indeed, the limit based on the thermal history of the IGM should be raised by a few factor. However, their final upper limit is mainly obtained from the reddening measurements of $z = 0.5$ supernovae Ia. Therefore, their conclusion would not be affected very much.

Bolton et al. (2008) suggested an inverted temperature–density relation in the lower density IGM at $z = 2$ –3 based on recent observations of the Lyman α forest in QSOs’ spectra. To explain this interesting phenomenon, we need a heating mechanism more efficient in a lower density medium. The dust photoelectric heating has such a property. Indeed, the dust heating rate even with the new yield model is a factor of 2 larger than the HeII photoionization heating rate in a medium with a density of 1/10 of the mean in the Universe at $z = 2$ if the dust-to-gas ratio is 1% of that in the Milky Way. Thus, the possibility of the dust heating is worth examining more in detail. For this

aim, the simple formula describing the dust photoelectric heating in the IGM presented in equation (16) will be very useful.

Finally, we have discussed the effect of the dust photoelectric heating in the early Universe. Before the cosmic reionization, the ionizing background radiation is not established, but there may be nonionizing UV background and X-ray background radiations. In the low temperature IGM only with a nonionizing UV background radiation, the dust photoelectric heating is not very efficient although it may be the strongest heating mechanism in the medium. In the partially ionized IGM with an X-ray background radiation, the HI photoionization heating rate is three orders of magnitude larger than the dust heating rate if the dust-to-gas ratio is 1% of that in the Milky Way. Therefore, we conclude that the dust photoelectric heating in the early Universe is not very important at least in the mean density environment.

We would appreciate comments from the reviewers, B. T. Draine and M. M. Abbas, which improve the quality of this paper very much. We are grateful to the conveners of the session “Cosmic Dust” in the 5th annual meeting of the Asia-Oceania Geosciences Society for organizing the interesting workshop. AKI is also grateful to all members of the Department of Physics, Nagoya University, especially the Ω Laboratory led by Tsutomu T. Takeuchi, for their hospitality during this work. AKI is supported by KAKENHI (the Grant-in-Aid for Young Scientists B: 19740108) by The Ministry of Education, Culture, Sports, Science and Technology (MEXT) of Japan.

References

- Abbas, M. M., et al., Photoelectric Emission Measurements on the Analogs of Individual Cosmic Dust Grains, *The Astrophys. J.*, **645**, 324–336, 2006.
- Abel, T., Haehnelt, M. G., Radiative Transfer Effects during Photoheating of the Intergalactic Medium, *The Astrophys. J. Letters*, **520**, L13–L16, 2001.
- Aguirre, A., Haiman, Z., Cosmological Constant or Intergalactic Dust? Constraints from the Cosmic Far-Infrared Background, *The Astrophys. J.*, **532**, 28–36, 2000.
- Aguirre, A., Hernquist, L., Katz, N., Gardner, J., Wein-

- berg, D., Enrichment of the Intergalactic Medium by Radiation Pressure-driven Dust Efflux, *The Astrophys. J. Letters*, **556**, L11–L14, 2001a.
- Aguirre, A., Hernquist, L., Schaye, J., Weinberg, D. H., Katz, N., Gardner, J., Metal Enrichment of the Intergalactic Medium at $z = 3$ by Galactic Winds, *The Astrophys. J.*, **560**, 599–605, 2001b.
- Aguirre, A., Hernquist, L., Schaye, J., Katz, N., Weinberg, D. H., Gardner, J., Metal Enrichment of the Intergalactic Medium in Cosmological Simulations, *The Astrophys. J.*, **561**, 521–549, 2001c.
- Alton, P. B., Davies, J. I., Bianchi, S., Dust outflows from starburst galaxies, *M.N.R.A.S.*, **343**, 51–63, 1999.
- Bendo, G. J., et al., The Spectral Energy Distribution of Dust Emission in the Edge-on Spiral Galaxy NGC 4631 as Seen with Spitzer and the James Clerk Maxwell Telescope, *The Astrophys. J.*, **652**, 283–305, 2006.
- Bertoldi, F., Carilli, C. L., Cox, P., Fan, X., Strauss, M. A., Beelen, A., Omont, A., Zylka, R., Dust emission from the most distant quasars, *Astronomy and Astrophysics*, **406**, L55–L58, 2003.
- Bianchi, S., Ferrara, A., Intergalactic medium metal enrichment through dust sputtering, *M.N.R.A.S.*, **358**, 379–396, 2005.
- Bolton, J. S., Viel, M., Kim, T.-S., Haehnelt, M. G., Carswell, R. F., Possible evidence for an inverted temperature-density relation in the intergalactic medium from the flux distribution of the Ly α forest, *M.N.R.A.S.*, **386**, 1131–1144, 2008.
- Corasaniti, P. S., The impact of cosmic dust on supernova cosmology *M.N.R.A.S.*, **372**, 191–198, 2006.
- Draine, B. T., Photoelectric heating of interstellar gas, *Astrophysical Journal Supplement Series*, **36**, 595–619, 1978
- Draine, B. T., Evolution of interstellar dust, in *The evolution of the interstellar medium*, Edited by L. Blitz, 193–205, Astronomical Society of the Pacific, San Francisco, 1990.
- Draine, B. T., Scattering by Interstellar Dust Grains. I. Optical and Ultraviolet, *The Astrophys. J.*, **598**, 1017–1025, 2003.
- Draine, B. T., Salpeter, E. E., Destruction mechanisms for interstellar dust, *The Astrophys. J.*, **231**, 438–455, 1979.
- Draine, B. T., Sutin, B., Collisional charging of interstellar grains, *The Astrophys. J.*, **320**, 803–817, 1987.
- Dwek, E., The Evolution of the Elemental Abundances in the Gas and Dust Phases of the Galaxy, *The Astrophys. J.*, **501**, 645–665, 1998.
- Elfgren, E., Désert, F.-X., Guiderdoni, B., Dust distribution during reionization, *Astronomy and Astrophysics*, **476**, 1145–1150, 2007.
- Fan, X., Carilli, C. L., Keating, B., Observational Constraints on Cosmic Reionization, *Annual Review of Astronomy & Astrophysics*, **44**, 415–462, 2006.
- Ferrarotti, A. S., Gail, H.-P., Composition and quantities of dust produced by AGB-stars and returned to the interstellar medium *Astronomy and Astrophysics*, **447**, 553
- Ferrara, A., Ferrini, F., Barsella, B., Franco, J., Evolution of dust grains through a hot gaseous halo, *The Astrophys. J.*, **381**, 137–146, 1991.
- Ferrara, A., Pettini, M., Shchekinov, Yu. A., Mixing metals in the early Universe, *M.N.R.A.S.*, **319**, 539–548, 2000.
- Fruchter, A., Krolik, J. H., Rhoads, J. E., X-Ray Destruction of Dust along the Line of Sight to γ -Ray Bursts, *The Astrophys. J.*, **563**, 597–610, 2001.
- Galli, D., Palla, F., The chemistry of the early Universe, *Astronomy and Astrophysics*, **335**, 403–420, 1998.
- Goobar, A., Bergström, L., Mörtzell, E., Measuring the properties of extragalactic dust and implications for the Hubble diagram, *Astronomy and Astrophysics*, **384**, 1–10, 2002.
- Gunn, J. E., Peterson, B. A., On the Density of Neutral Hydrogen in Intergalactic Space, *The Astrophys. J.*, **142**, 1633–1641, 1965.
- Haardt, F., Madau, P., Radiative Transfer in a Clumpy Universe. II. The Ultraviolet Extragalactic Background, *The Astrophys. J.*, **461**, 20–37, 1996.
- Hirashita, H., Nozawa, T., Kozasa, T., Ishii, T. T., Takeuchi, T. T., Extinction curves expected in young galaxies, *M.N.R.A.S.*, **357**, 1077–1087, 2005.
- Hirashita, H., Nozawa, T., Takeuchi, T. T., Kozasa, T., Extinction curves flattened by reverse shocks in supernovae, *M.N.R.A.S.*, **384**, 1725–1732, 2005.
- Hui, L., Gnedin, N. Y., Equation of state of the photoionized intergalactic medium, *M.N.R.A.S.*, **292**, 27–42, 1997.
- Inoue, A. K., and Kamaya, H., Constraint on intergalactic dust from thermal history of intergalactic medium, *M.N.R.A.S.*, **341**, L7–L11, 2003.
- Inoue, A. K., and Kamaya, H., Amount of intergalactic dust: constraints from distant supernovae and the thermal history of the intergalactic medium, *M.N.R.A.S.*, **350**, 729–744, 2004.
- Jones, A. P., Tielens, A. G. G. M., Hollenbach, D. J., Grain Shattering in Shocks: The Interstellar Grain Size Distribution, *The Astrophys. J.*, **469**, 740–764, 1996.
- Loeb, A., Barkana, R., The Reionization of the Universe by the First Stars and Quasars, *Annual Review of Astronomy and Astrophys.*, **39**, 19–66, 2001.
- Mathis, J. S., Rumpl, W., and Nordsieck, K. H., The size distribution of interstellar grains, *Astrophys. J.*, **217**, 425–433, 1977.
- Maiolino, R., Schneider, R., Oliva, E., Bianchi, S., Ferrara, A., Mannucci, F., Pedani, M., Roca Sogorb, M., A supernova origin for dust in a high-redshift quasar, *Nature*, **431**, 533–535, 2004.

- Montier, L. A., Giard, M., The importance of dust in cooling and heating the InterGalactic Medium, *Astronomy and Astrophysics*, **417**, 401–409, 2004.
- Nath, B. B., Sethi, S. K., and Shchekinov, Y., Photoelectric heating for dust grains at high redshifts, *M.N.R.A.S.*, **303**, 1–14, 1999.
- Nozawa, T., Kozasa, T., Umeda, H., Maeda, K., Nomoto, K., Dust in the Early Universe: Dust Formation in the Ejecta of Population III Supernovae, *The Astrophys. J.*, **598**, 785–803, 2003.
- Nozawa, T., Kozasa, T., Habe, A., Dwek, E., Umeda, H., Tomimaga, N., Maeda, K., Nomoto, K., Evolution of Dust in Primordial Supernova Remnants: Can Dust Grains Formed in the Ejecta Survive and Be Injected into the Early Interstellar Medium?, *The Astrophys. J.*, **598**, 955–966, 2007.
- Osterbrock, D. E., Ferland, G. J., in *Astrophysics of Gaseous Nebulae and Active Galactic Nuclei Second Edition*, University Science Books, San Salito California, 2006.
- Rho, J., Kozasa, T., Reach, W. T., Smith, J. D., Rudnick, L., DeLaney, T., Ennis, J. A., Gomez, H., Tappe, A., Freshly Formed Dust in the Cassiopeia A Supernova Remnant as Revealed by the Spitzer Space Telescope, *The Astrophys. J.*, **673**, 271–282, 2008.
- Scott, J., Bechtold, J., Dobrzycki, A., Kulkarni, V. P., A Uniform Analysis of the Ly α Forest at $z = 0 - 5$. II. Measuring the Mean Intensity of the Extragalactic Ionizing Background Using the Proximity Effect, *The Astrophys. J. Suppl.*, **130**, 67–89, 2000.
- Spitzer, L. Jr., The Dynamics of the Interstellar Medium. II. Radiation Pressure, *The Astrophys. J.*, **94**, 232–244, 1941.
- Venkatesan, A., Giroux, M. L., Shull, J. M., Heating and Ionization of the Intergalactic Medium by an Early X-Ray Background, *The Astrophys. J.*, **563**, 1–8, 2001.
- Weingartner, J., and Draine, B. T., Photoelectric Emission from Interstellar Dust: Grain Charging and Gas Heating, *The Astrophys. J. Suppl.*, **134**, 263–281, 2001.
- Weingartner, J., Draine, B. T., and Barr, D. K., Photoelectric Emission from Dust Grains Exposed to Extreme Ultraviolet and X-Ray Radiation, *The Astrophys. J.*, **645**, 1188–1197, 2006.
- Williams, B. J., et al., Dust Destruction in Fast Shocks of Core-Collapse Supernova Remnants in the Large Magellanic Cloud, *The Astrophys. J. Letters*, **652**, L33–L56, 2006.
- Xilouris, E., Alton, P., Alikakos, J., Xilouris, K., Boumis, P., Goudis, C., Abundant Dust Found in Intergalactic Space, *The Astrophys. J. Letters*, **651**, L107–L110, 2008.
- Yamada, K., Kitayama, T., Infrared Emission from Intracluster Dust Grains and Constraints on Dust Properties, *Publications of the Astronomical Society of Japan*, **57**, 611–619, 2005.
- Yun, M. S., Ho, P. T. P., Lo, K. Y., A High-Resolution Image of Atomic Hydrogen in the M81 Group of Galaxies, *Nature*, **372**, 530–532, 1994.
- Zhang, P., Corasaniti, P. S., Cosmic Dust Induced Flux Fluctuations: Bad and Good Aspects, *The Astrophys. J.*, **657**, 71–75, 2007.

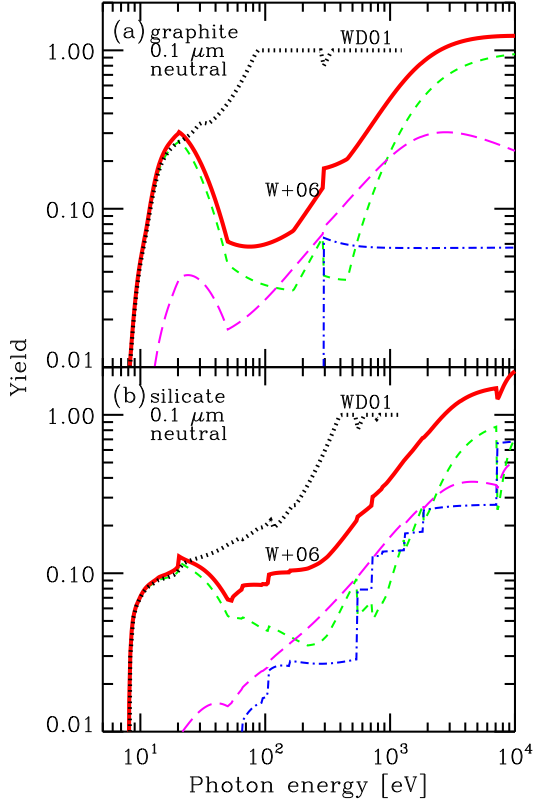


Figure 1: Photoelectric yield models of $0.1 \mu\text{m}$ neutral (a) graphite and (b) silicate grains. The dotted lines are the WD01 model (Weingartner & Draine 2001) and the solid lines are the W+06 model (Weingartner et al. 2006). The W+06 model consists of three processes: the primary photoelectron emission (short dashed line), the secondary electron emission (long dashed line), and the Auger electron emission (dot-dashed line).

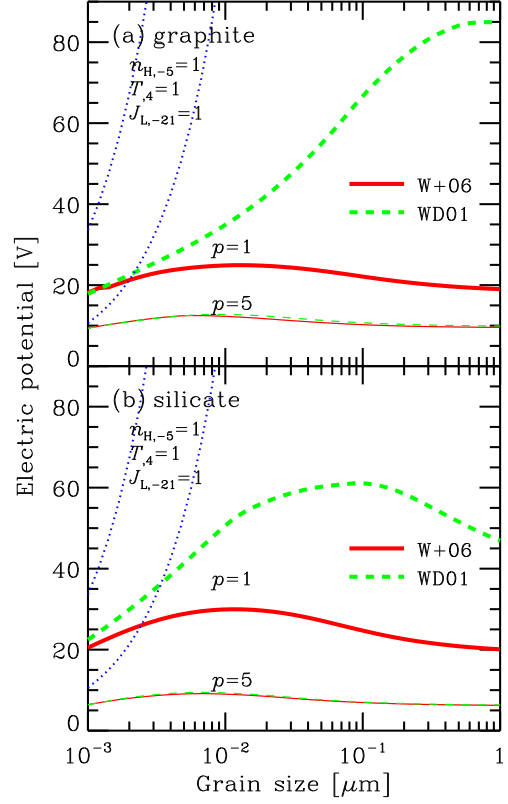


Figure 2: Equilibrium electric potential as a function of grain size: (a) graphite and (b) silicate. The solid lines are the W+06 model and the dashed lines are the WD01 model. The thick lines are the case with the spectral index of the radiation field $p = 1$ and the thin lines are the case with $p = 5$. Other assumed quantities are noted in the panels as the hydrogen density $n_{\text{H},-5} = n_{\text{H}}/10^{-5} \text{ cm}^{-3}$, the gas temperature $T_{,4} = T/10^4 \text{ K}$, and the radiation intensity $J_{\text{L},-21} = J_{\text{L}}/10^{-21} \text{ erg s}^{-1} \text{ cm}^{-2} \text{ Hz}^{-1} \text{ sr}^{-1}$. The dotted lines show the critical electric potential where the grain destruction occurs by the Coulomb explosion; the upper lines are the case with the tensile strength of $10^{11} \text{ dyn cm}^{-2}$ and the lower lines are the case with $10^{10} \text{ dyn cm}^{-2}$.

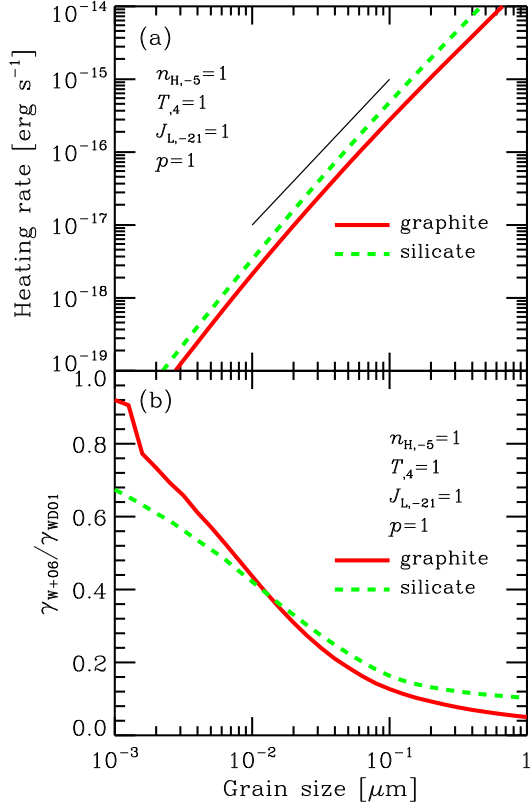


Figure 3: Photoelectric heating rate per a grain as a function of grain size: (a) heating rate with the W+06 yield model and (b) ratio of the heating rate with the W+06 yield model to that with the WD01 yield model. The solid lines are the graphite case and the dashed lines are the silicate case. The assumed quantities are noted in the panels as the hydrogen density $n_{\text{H},-5} = n_{\text{H}}/10^{-5} \text{ cm}^{-3}$, the gas temperature $T_{,4} = T/10^4 \text{ K}$, the radiation intensity $J_{\text{L},-21} = J_{\text{L}}/10^{-21} \text{ erg s}^{-1} \text{ cm}^{-2} \text{ Hz}^{-1} \text{ sr}^{-1}$, and the spectral index of the radiation field $p = 1$. The thin solid line in the panel (a) shows the slope proportional to the square of size.

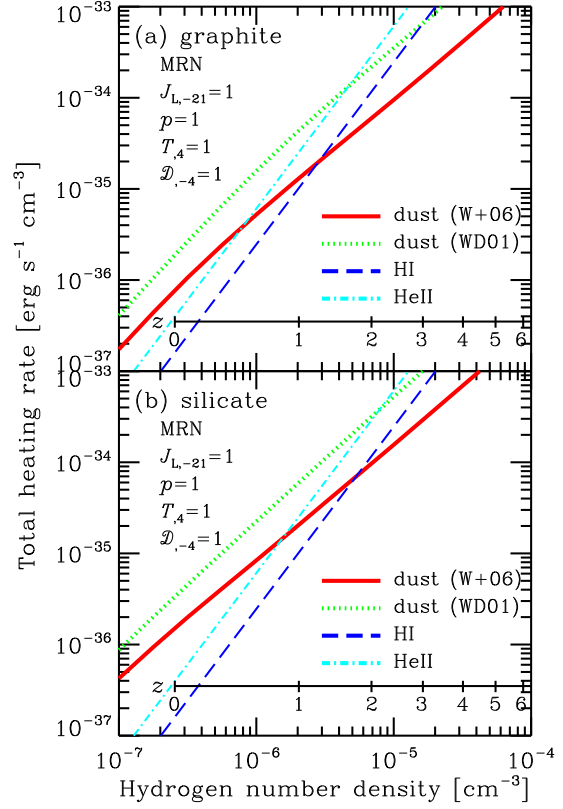


Figure 4: Photoelectric heating rates as a function of hydrogen number density: (a) graphite and (b) silicate. The solid lines are the W+06 model and the dotted lines are the WD01 model. The assumed grain size distribution is the so-called MRN distribution (Mathis, Rumpl, & Nordsieck 1977). Other assumed quantities are noted in the panels as the gas temperature $T_{,4} = T/10^4 \text{ K}$, the radiation intensity $J_{\text{L},-21} = J_{\text{L}}/10^{-21} \text{ erg s}^{-1} \text{ cm}^{-2} \text{ Hz}^{-1} \text{ sr}^{-1}$, the spectral index of the radiation field p , and the dust-to-gas mass ratio $\mathcal{D}_{,-4} = \mathcal{D}/10^{-4}$. The dashed lines are the HI photoionization heating rate and the dot-dashed lines are the HeII photoionization heating rate with assuming the ionization equilibrium. We also show the redshift at which the number density on the horizontal axis corresponds to the mean density of the Universe.

Table 1: Possible size distributions of the intergalactic dust.

MRN	Mathis, Rumpl, & Nordsieck (1977)
single power law ^a	
q	3.5
a_{\min}	50 Å
a_{\max}	0.25 μm
$\langle a \rangle$	350 Å
BF05	Bianchi & Ferrara (2005)
single power law ^a	
q	3.5
a_{\min}	0.1 μm
a_{\max}	0.25 μm
$\langle a \rangle$	0.16 μm
N03	Nozawa et al. (2003)
double power law ^b	
$q_1 (a \leq a_c)$	2.5
$q_2 (a > a_c)$	3.5
a_{\min}	2 Å
a_{\max}	0.3 μm
a_c	0.01 μm
$\langle a \rangle$	290 Å
N07	Nozawa et al. (2007)
double power law ^b	
$q_1 (a \leq a_c)$	1.0
$q_2 (a > a_c)$	2.5
a_{\min}	10 Å
a_{\max}	0.3 μm
a_c	0.01 μm
$\langle a \rangle$	0.12 μm
SG	—
single power law ^a	
q	3.5
a_{\min}	50 Å
a_{\max}	0.025 μm
$\langle a \rangle$	110 Å

^a The grain size distribution $n(a) \propto a^{-q}$.

^b The grain size distribution $n(a) \propto a^{-q_1}$ for $a \leq a_c$ and $\propto a^{-q_2}$ for $a > a_c$.

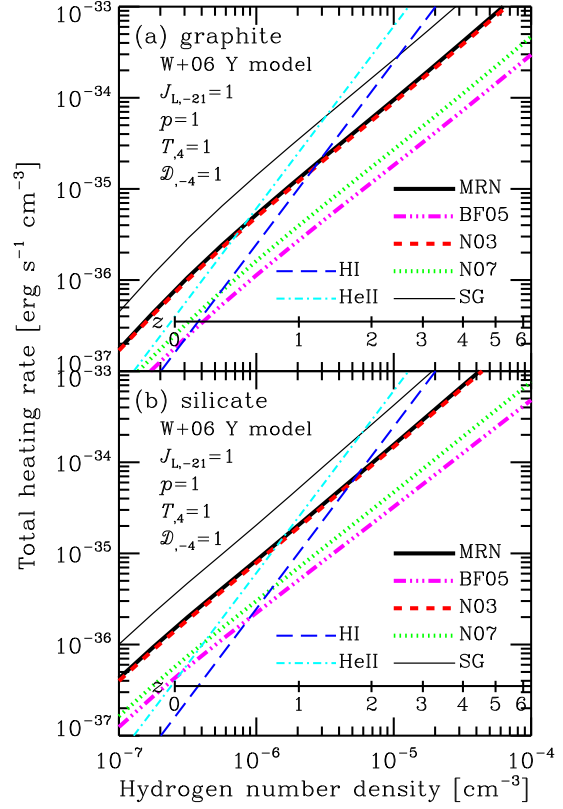


Figure 5: Same as Fig. 4 but for various size distribution functions with the W+06 yield model: (a) graphite and (b) silicate. The thick solid lines are the MRN case. The short-dashed lines are the size distribution expected from the grain formation model in supernova ejecta by Nozawa et al. (2003). The dotted lines are the size distribution expected after the grain destruction by the reverse shock in the supernova remnant by Nozawa et al. (2007). The triple-dot-dashed lines are the MRN but only size larger than 0.1 μm because of a filtering effect in the transfer of grains from galaxies to the IGM suggested by Bianchi & Ferrara (2005). The thin solid lines are the MRN but only size smaller than 250 Å as a comparison. The dashed and dot-dashed lines are HI and HeII heating rates.

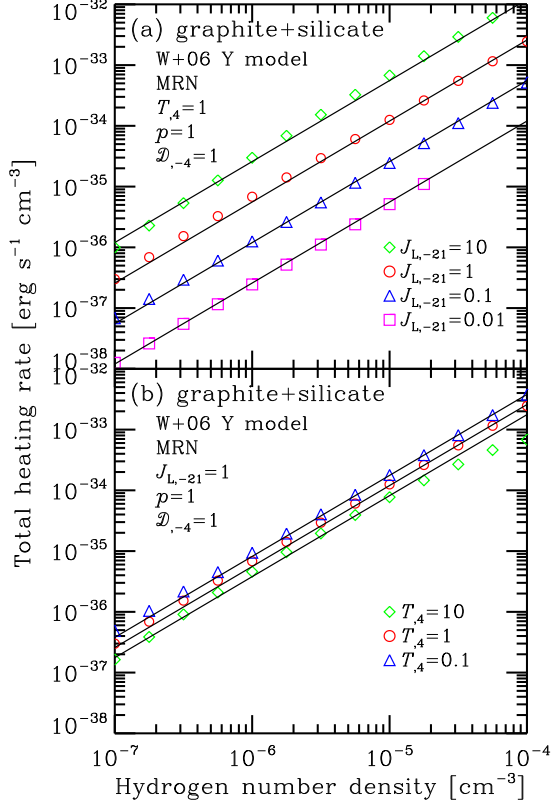


Figure 6: Same as Fig. 4 but for various settings. The photoelectric yield model is the W+06 model. We assume that the dust consists of a mixture of graphite and silicate (50% each in mass) with the MRN size distribution. (a) Different intensities at the Lyman limit of the radiation field: $J_L/10^{-21} \text{ erg s}^{-1} \text{ cm}^{-2} \text{ Hz}^{-1} \text{ sr}^{-1} = 10$ (diamonds), 1 (circles), 0.1 (triangles), and 0.01 (squares). (b) Different temperatures of the gas: $T/10^4 \text{ K} = 10$ (diamonds), 1 (circles), and 0.1 (triangles). Other assumed quantities are noted in the panels. See the caption of Fig. 4 for the notation. The solid lines are the simple formula shown in eq. (16).

Table 2: Photoelectric heating in the early Universe.

Common setting	
z	10
n_H	$3 \times 10^{-4} \text{ cm}^{-3}$
\mathcal{D}	10^{-4}
size distribution	MRN
J_L	$1 \times 10^{-21} \text{ erg s}^{-1} \text{ cm}^{-2} \text{ Hz}^{-1} \text{ sr}^{-1}$
p	1
$E_{\text{UV}}^{\text{max}}$	13.6 eV
Nonionizing UV only	
T	30 K
x_e	10^{-4}
Γ_{pe}	$7 \times 10^{-36} \text{ erg s}^{-1} \text{ cm}^{-3}$
t_{pe}	$9 \times 10^9 \text{ yr}$
With X-ray background	
E_X^{min}	300 eV
T	10^4 K
x_e	0.3
Γ_{pe}	$2 \times 10^{-33} \text{ erg s}^{-1} \text{ cm}^{-3}$
$\Gamma_{\text{pi,X}}^{\text{HI}}$	$2 \times 10^{-30} \text{ erg s}^{-1} \text{ cm}^{-3}$